Supplemental Material

Radioactive GLP-1r tracer synthesis and quality control

Briefly, ^{68}Ga was produced daily by automatic elution of a chemical grade generator (iThema Labs, DSD-Pharma, Austria) with 6 ml 0.6M HCL Suprapure (ABX, HCL-101) as part of the synthesis process. Throughout the period when experiments were conducted, the generator was eluted daily to maintain the capacity of the tin dioxide polyethylene column to retain ^{68}Ge from the eluate. Production of [^{68}Ga]Ga-DO3A-VS-Cys40-Exendin-4 was achieved using a ^{68}Ga-peptide synthesis cassette (ABX Scintomics, SC-1, Germany) with 47 μg of the DO3A-VS-Cys40-Exendin-4 cold molecule (CSBio peptide, USA) dissolved in 2.5 ml Hepes buffer (Sigma, France) inserted in the reactor. The synthesizer sequence (Scintomics GRP, Germany) was modified to (a) adjust for the temperature and heating duration of the reactor, (b) allow for extended tubing between the reactor and the final vial containing the radioactive compound and (c) reduce the volume of phosphate buffer from 15 to 5 ml as a consequence of the final filtration step removal without affecting the final pH (pH = 7.4).

Prior to injection, the final compound was checked for the amount of ^{68}Ga that was not associated with Exendin-4 and the concentration of Exendin-4 labeled by ^{68}Ga in solution, using high-performance chromatography. The system comprised two Knauer pumps for high-pressure gradient elution of the end-capped analytic column (Luna C18(2), Phenomenex, USA) associated with a UV detector (220 nm, Knauer, Germany) and a radiation flow detector (Flow-RAM, LabLogic, UK) in series. The gradient conditions were as follows: solvent A 10 mM trifluoroacetic acid; solvent B 70% acetonitrile, 30% H$_2$O, and 10 mM trifluoroacetic acid with UV detection at 220 nm; gradient elution was done for 0–2 min at 35% B, 2–9 min at 35%–100% B, and 9–12 min at 100% solvent B; and the flow rate was 2.0 mL/min. Data processing was performed with ChromStar (Scpa, Germany) and included baseline drift removal as a consequence of the acetonitrile gradient. [^{68}Ga]Ga-DO3A-VS-Cys40-Exendin-4 was eluted with a retention time of ~5.1 min. The radioactivity of the final compound was calculated before injection using a dose calibrator (MP-DC01- Mec Murphill, Italy).

Arterial Input function measurement

Blood was drawn from the artery and re-injected into the vein at a rate of 8.0 ± 0.1 mL/min through a peristaltic pump controlled by an artificial intelligence algorithm (Labview 17, USA)

receiving the flow signal from a transit-time ultrasonic probe clipped onto the loop tubing (Transonic, Emka Technologies, France). Arterial blood was also sampled at 10-minute intervals with a blood sampler (Instech, Phymep, France) connected to the loop after the radioactivity probe. The radioactivity of whole blood and plasma samples was measured using a gamma counter (Wizard 1470, Perkin Elmer, France). The in-line sampling device and the gamma counter were cross-calibrated on a daily basis after the experiment against the PET scanner using a ^{68}Ga water-filled phantom of 4 L. In addition, data originating from the in-line blood sampler were corrected for dispersion caused by the length of the arterial sampling line according to Munk et al. [1].

[^{68}Ga]Ga-DO3A-VS-Cys40-Exendin-4 Displacement studies

Three additional animals, all weighing 34 kg, were used only for displacement studies to ascertain the specificity of the portal GLP-1r binding. The imaging procedure was identical to that described above, but included only one CT imaging procedure for attenuation purposes for the PET image. The procedure lasted ~8 hours and comprised 3 sequential co-administrations of the radioactive tracer (0.2MBq/Kg) with escalating doses of unlabeled DO3A-Exendin-4 (1, 5 and 10 µg/kg). Each dose was injected at least 3 hours after the previous one.

Because the specificity of the [^{68}Ga]Ga-DO3A-VS-Cys40-Exendin-4 for labeling GLP-1r, while already investigated in the porcine pancreas, has not been established at the portal level, an additional displacement study was performed on three additional lean pigs using co-injection of cold tracer in an escalating scheme. Portal and pancreas binding potentials followed the same pattern i.e. a steady decrease during escalating doses of the unlabeled agonist. At 1µg/kg, pancreatic and portal binding merged and could not be distinguished further with larger doses of the agonist (Supplemental Figure 1). For both organs, this pattern confirmed than the majority of the tracer uptake involved specific GLP-1r binding and that the dose of [^{68}Ga]Ga-DO3A-VS-Cys40-Exendin-4 was within the requirements for tracer boundaries.

Supplemental Figure 1

Kinetic analysis of [^{68}Ga]Ga-DO3A-VS-Cys40-Exendin-4

Data were fitted to a 2-tissue compartment model with Akaike and Bayesian information criteria (unitless) as an indicator of the adequacy of the model. The compound parameter Vs (Specific volume of distribution) describes the binding potential [2] for this kinetic model. Vt is

also presented in the manuscript to identify the total volume of distribution (specific and non-specific binding). The appropriateness of the two compartments model was investigated in comparison with a single compartment analysis and a spectral analysis as suggested by Gunn et al (3). These analyses were also performed using PMod 3.9. The results of this comparison are given in Supplemental table 1 together with the putative biological meaning of the compartments and the micro-constants according to Innis et al (2). PET images were also converted and coded, voxel wise, in units of binding potential (ml/ccm) using a Logan plot for representation purposes.

Supplemental Figure 2 and 3

Supplemental Table 1

Positioning of the stimulating electrode along the portal vein

The animals were anesthetized and surgically prepared for dissection of the cervical vagus as described (4), (5). Minimally invasive laparoscopic access to the abdomen was performed to insert intra-mural stimulating electrodes used to identify portal neurons. Four electrodes, comprising Ag-Ag-Cl wires (Phymep, France) 40 mm in length, were inserted in the connective tissue surrounding the portal vein along its long axis so that one electrode was positioned in each of the 90° quadrants. The area used for electrode placement was adapted, for each animal, based on the prior multimodal (PET and injected and non-injected CT) imaging of the portal vein, so that the electrodes were located where the density of GLP-1r was maximal. Vt values were calculated along the length of portal vein and a segment 40 mm length centered on maximal Vt identified. The CT and the area of interest were then loaded onto a three-dimensional surgical navigation system (6) co-registered with the CT fiducial markers. The position of the stimulating electrodes was identified by navigating the abdominal cavity using infra-red optical probes (NDI Polaris, USA) located on the locally built electrode implantation tool and referenced to the navigation system (NDI architect software, USA).

Evaluation of the current density during field stimulation probing

Once the cervical pool was constructed and filled with paraffin, the impedance of the stimulating electrodes placed during the abdominal laparoscopic procedure was measured both for their real and imaginary parts. This delay was necessary for abdominal fluid extravasation, if any, to take place and to stabilize the impedance after electrode placement. The impedance

between the two field stimulating electrodes and between the electrodes and a reference electrode was measured using a purpose-made device comprising a programmable current stimulator and a fully isolated A/D card (NI-USB 621, NI, USA) connected in parallel with the stimulator output. The voltage drop across a precision 1KOhm resistor was also measured using the same A/D card. The current stimulator was able to generate 1ms current pulses from 0.1 to 2.5 mA with 0.1 mA step. Both were connected to a computer running a specialized software running under Labview 2011. Tension and current mirror occurring during a total of 20 pulses with an amplitude step of 0.1 mA were recorded at 10 kHz sample frequency and analyzed with a Randles equivalent circuit (Warburg impedance was assumed to be negligible) (7), (5).

The impedance data, together with a simplified model of the portal area obtained by spatial filtering of the portal vein's 3D representation, were imported into Comsol Multiphysics modeling software (Comsol Inc, USA). The finite element method was used to evaluate the current density along the portal vein and its vicinity (8). The STL file representing the portal vein and obtained from the injected CT imaging was simplified using a spatial Gaussian filter. Above 1.5 Million tetrahedral elements, the computing process required to solve the equations became unstable and failed to get an operational solution. The normalized electric field below 1V/mm, i.e., unable to trigger action potential irrespective of the neuron's conduction speed, was found as close as 10 mm from the portal wall, suggesting that « en passant » stimulation was not possible for vagal branches located nearby the portal electrodes. The primary factor involved in the rapid decay of the current density was the large in-parallel conductance rather than the value of the in-series resistance itself.

Vagal afferent recording

The left cervical vagus freed from surrounding connective and fat tissues and the skin and cervical muscles were sutured to a metallic frame to create a pool filled with warm paraffin oil. Recordings were performed after the section of the cervical vagus and micro-dissection of its distal end under a stereomicroscope. Adequate amplification of the signal was provided by a purpose-made AC amplifier placed near the recording electrode (tungsten wire, 50 µm, WPI USA). Neurons with evoked action potentials during portal electrical stimulation were selected by microdissection of the vagal bundle. Vagal activity was continuously recorded at 22 kHz after low pass (0.03 s) and high pass (12 kHz) filtration using custom-made software written under Labview language (National Instruments, USA). Raw data were analyzed for changes in the firing rate after transfer to Spike2 (CED, England, UK). Spikes were extracted from

background noise based on their overall shapes using the semi-automatic classification method built-in Spike2.

Phenotypic characterization

The animals were scanned by CT (Discovery ST, General Electric Medical Systems, France) to quantify subcutaneous and abdominal fat volumes that were obtained after averaging CT slices performed at T13 and L2 levels (9). Segmentation of subcutaneous and intra-abdominal fat was performed semi-automatically using ITK-Snap. Total abdominal fat was estimated as the sum of subcutaneous and intra-abdominal fat (5).

Insulin sensitivity was measured using a euglycemic-hyperinsulinemic clamp performed after the completion of the imaging procedure and using the same catheters as those employed for GLP-1r quantification (10). Insulin (Actrapid, Novo Nordisk, Denmark) and 20% glucose were infused in the saphenous vein. Insulin was diluted in 50 ml saline plus 0.5% homologous blood and infused at $120mU.kg^{-1}.hr^{-1}$ without a priming dose. Arterial blood samples were obtained from the femoral artery every 5 min and measured by the glucose oxidase method on a rapid analyzer (Analox GM9 Analyzer; Analox Instruments, UK). For each clamp, the plateau was considered to have been achieved when differences in glucose uptake rate and glycemia were less than 5% in three consecutive samples. In most animals, this was reached within two hours of the onset of the clamp. Plasma insulin concentrations were measured using a ST-AIA-Pack IRI reagent kit, with a quantification limit of 0.5 $\mu U.ml^{-1}$ and intra-assay coefficient of variation less than 2% from 12 to 200 $\mu U.ml^{-1}$.

At the completion of the clamp procedure, the glucose infusion was reduced progressively over 30 minutes to avoid hypoglycemia. While the animals were still anesthetized, the femoral catheter was removed using an aseptic procedure and replaced by an arterial closure device that maintains arterial competence while immediately preventing blood leakage (Angio-Seal, St. Jude Medical, France). The venous catheters were also withdrawn prior to the return of the animals to their cages.

References

1.   Munk OL, Keiding S, Bass L: A method to estimate dispersion in sampling catheters and to calculate dispersion-free blood time-activity curves. *Med Phys* 35:3471-3481, 2008

2.   Innis RB, Cunningham VJ, Delforge J, Fujita M, Gjedde A, Gunn RN, Holden J, Houle S, Huang S-C, Ichise M: Consensus nomenclature for in vivo imaging of reversibly binding radioligands. *Journal of Cerebral Blood Flow & Metabolism* 27:1533-1539, 2007

3.   Gunn RN, Gunn SR, Turkheimer FE, Aston JA, Cunningham VJ: Positron emission tomography compartmental models: a basis pursuit strategy for kinetic modeling. *J Cereb Blood Flow Metab* 22:1425-1439, 2002

4.   Cuche G, Blat S, Malbert CH: Desensitization of ileal vagal receptors by short-chain fatty acids in pigs. *American Journal of Physiology- Gastrointestinal and Liver Physiology* 280:G1013-21, 2001

5.   Malbert CH, Bobillier E, Picq C, Divoux JL, Guiraud D, Henry C: Effects of chronic abdominal vagal stimulation of small-diameter neurons on brain metabolism and food intake. *Brain Stimul* 10:735-743, 2017

6.   Askeland C, Solberg OV, Bakeng JBL, Reinertsen I, Tangen GA, Hofstad EF, Iversen DH, Våpenstad C, Selbekk T, Langø T, Hernes TAN, Olav Leira H, Unsgård G, Lindseth F: CustusX: an open-source research platform for image-guided therapy. *International Journal of Computer Assisted Radiology and Surgery* 11:505-519, 2016

7.   Wei XF, Grill WM: Impedance characteristics of deep brain stimulation electrodes in vitro and in vivo. *J Neural Eng* 6:046008, 2009

8.   Dali M, Rossel O, Andreu D, Laporte L, Hernández A, Laforet J, Marijon E, Hagège A, Clerc M, Henry C, Guiraud D: Model based optimal multipolar stimulation without a priori knowledge of nerve structure: application to vagus nerve stimulation. *J Neural Eng* 15:046018, 2018

9.   Val-Laillet D, Blat S, Louveau I, Malbert CH: A computed tomography scan application to evaluate adiposity in a minipig model of human obesity. *Br J Nutr* 104:1719-1728, 2010

10.   Malbert C-H, Horowitz M, Young RL: Low-calorie sweeteners augment tissue-specific insulin sensitivity in a large animal model of obesity. *European journal of nuclear medicine and molecular imaging* 1-12, 2019

Supplemental table 1:   Changes in K1 and Vt values depending on the modelling strategies

	Lean		Obese	
	K1	**Vt**	**K1**	**Vt**
2 compartments	1.06 ± 0.271	4.80 ± 0.139	0.24 ± 0.051*	2.42 ± 0.074‡
1 compartment	1.57 ± 0.334	3.72 ± 0.177	0.53 ± 0.143*	2.51 ± 0.191‡
Spectral analysis	1.05 ± 0.235	5.10 ± 0.483	0.40 ± 0.026*	3.18 ± 0.165‡

* different from Lean at $p<0.05$, ‡ different from Lean at $p<0.05$
K1 micro-constant is displayed only since it is present in all analysis models.
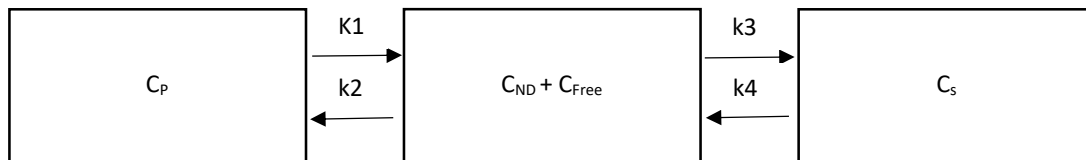
C_P - plasma concentration of 68Ga-Ga-DO3A-VS-Cys40-Exendin-4
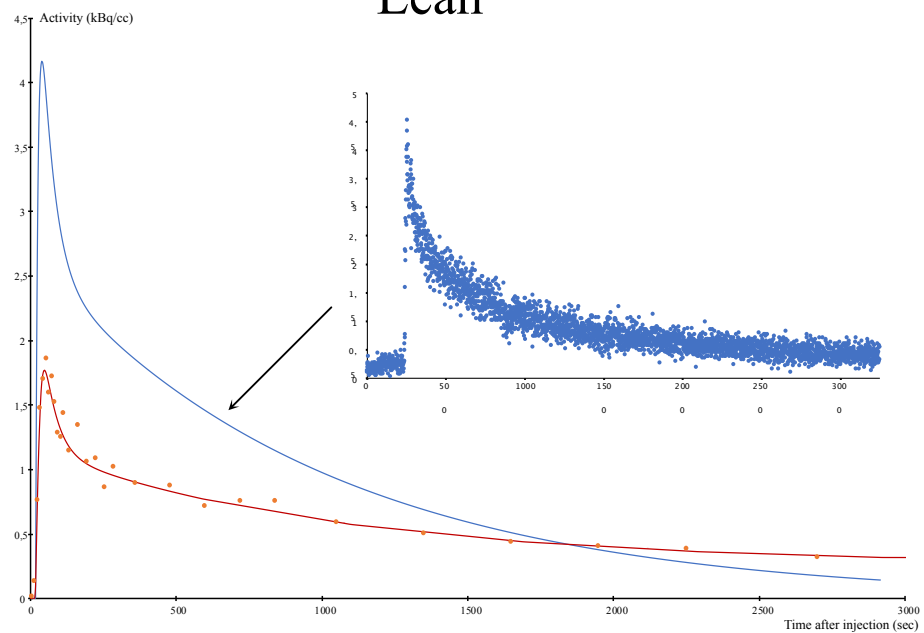C_{ND} - Concentration of the non-displaceable fraction
C_{Free} - Concentration of the free fraction
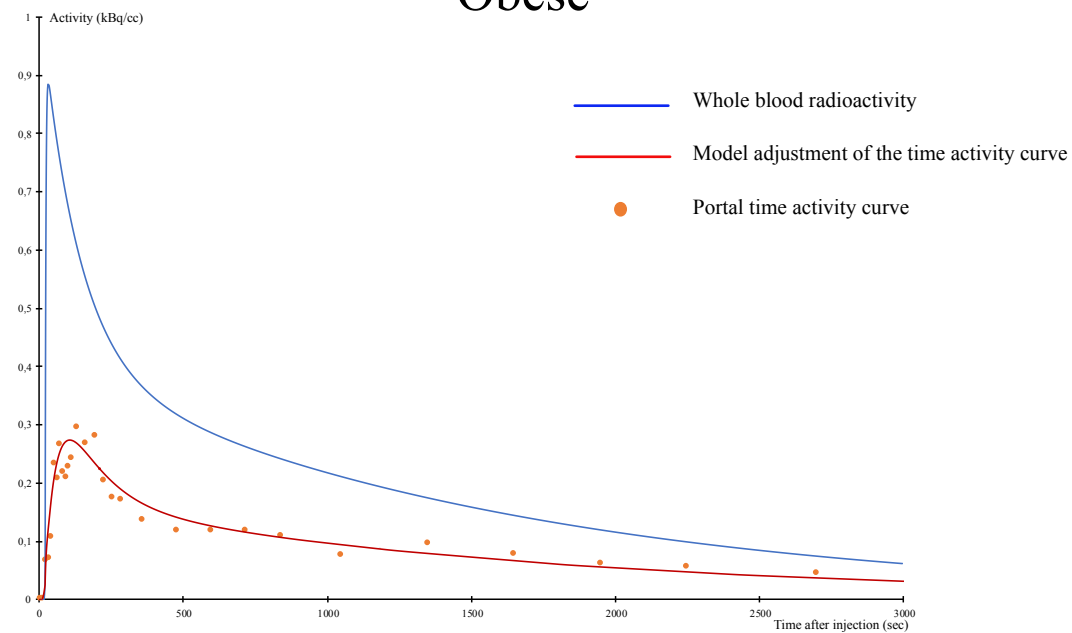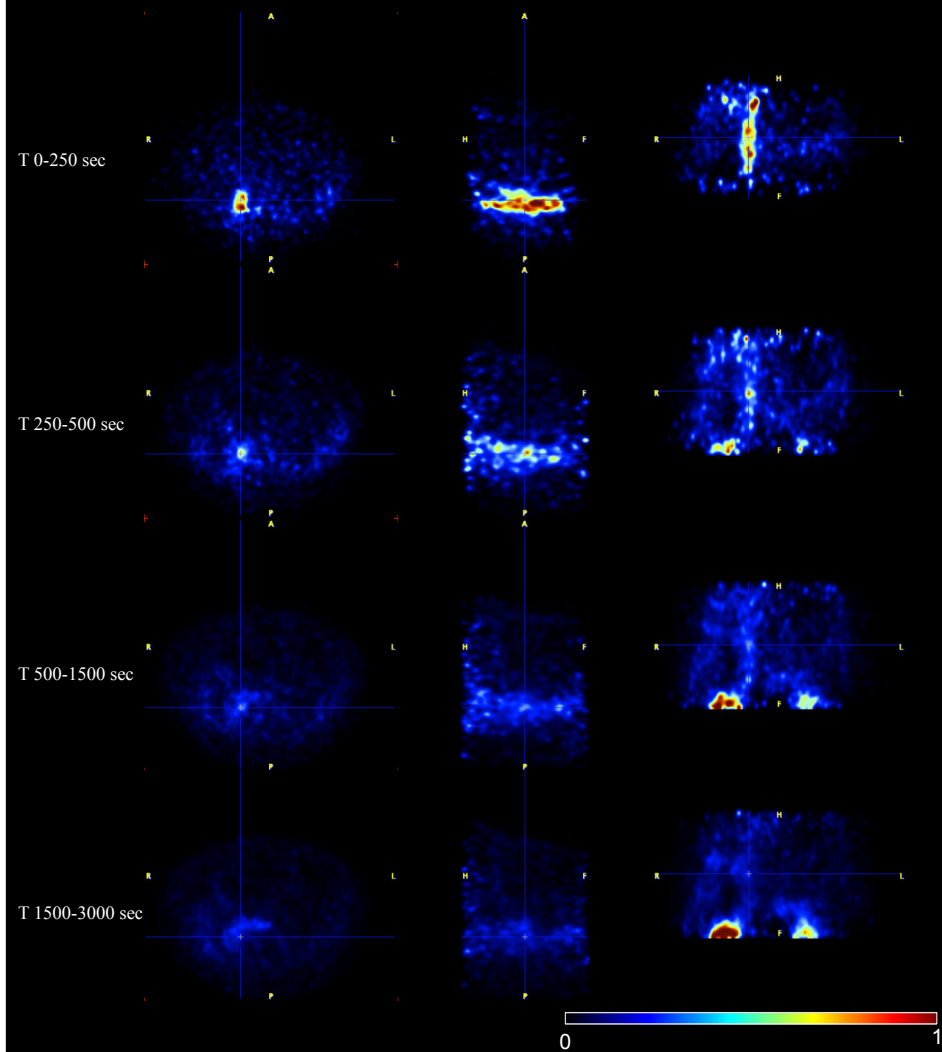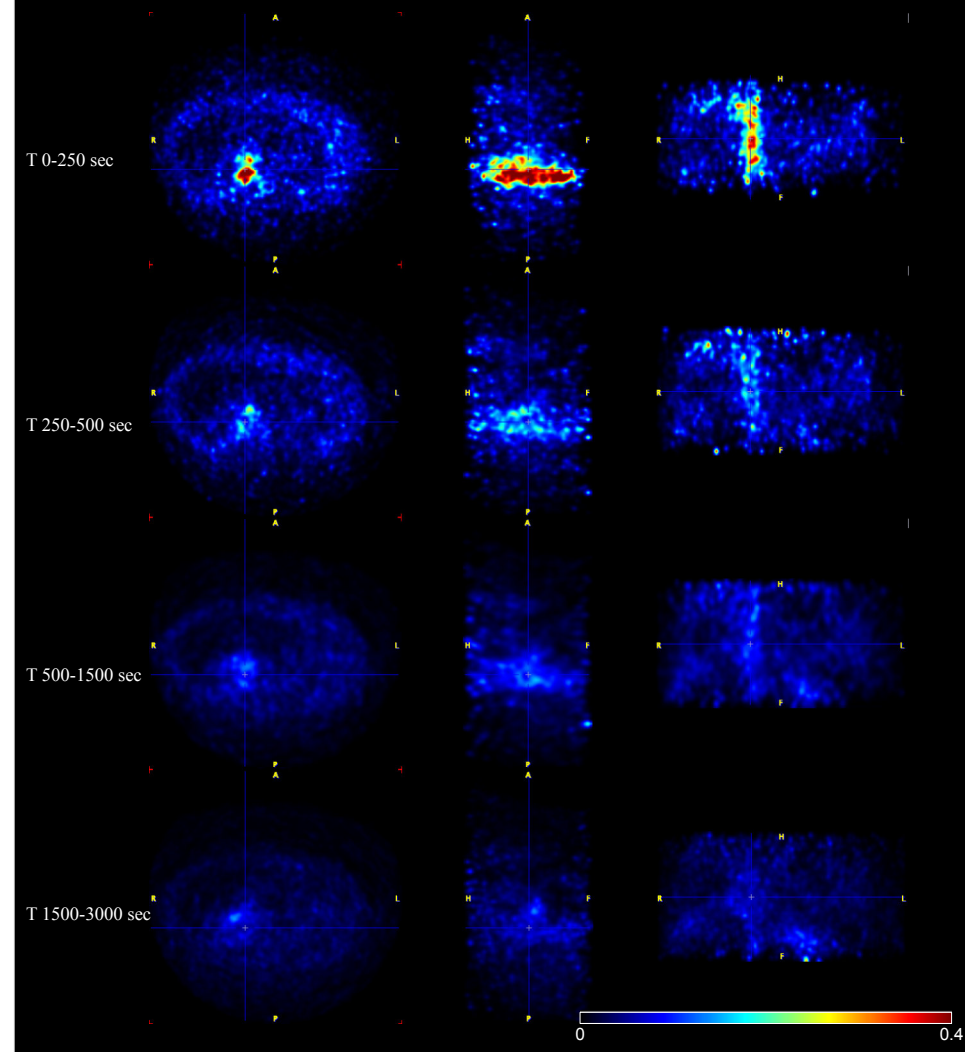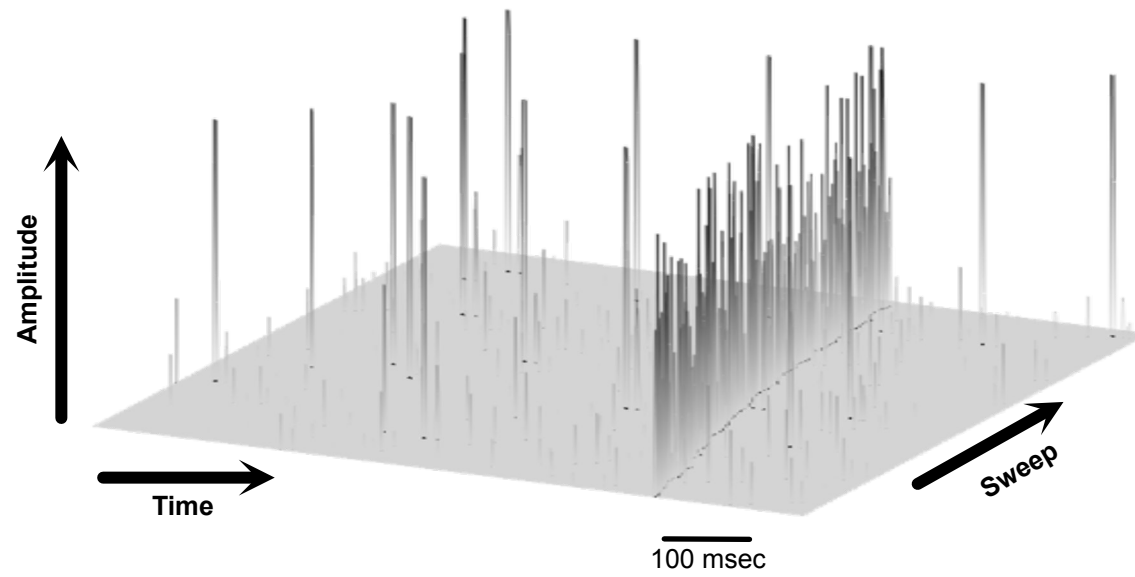C_S - Concentration of the specifically bound fraction i.e. attached to GLP1r

Lean

Activity (kBq/cc)

Time after injection (sec)

Obese

Activity (kBq/cc)

Time after injection (sec)

Whole blood radioactivity

Model adjustment of the time activity curve

Portal time activity curve

Lean

Obese

A

100 µV

100 msec

B

Amplitude

Time

Sweep

100 msec

Lean

Obese

Sup pancreatico-duodenal vein

Gastric veins
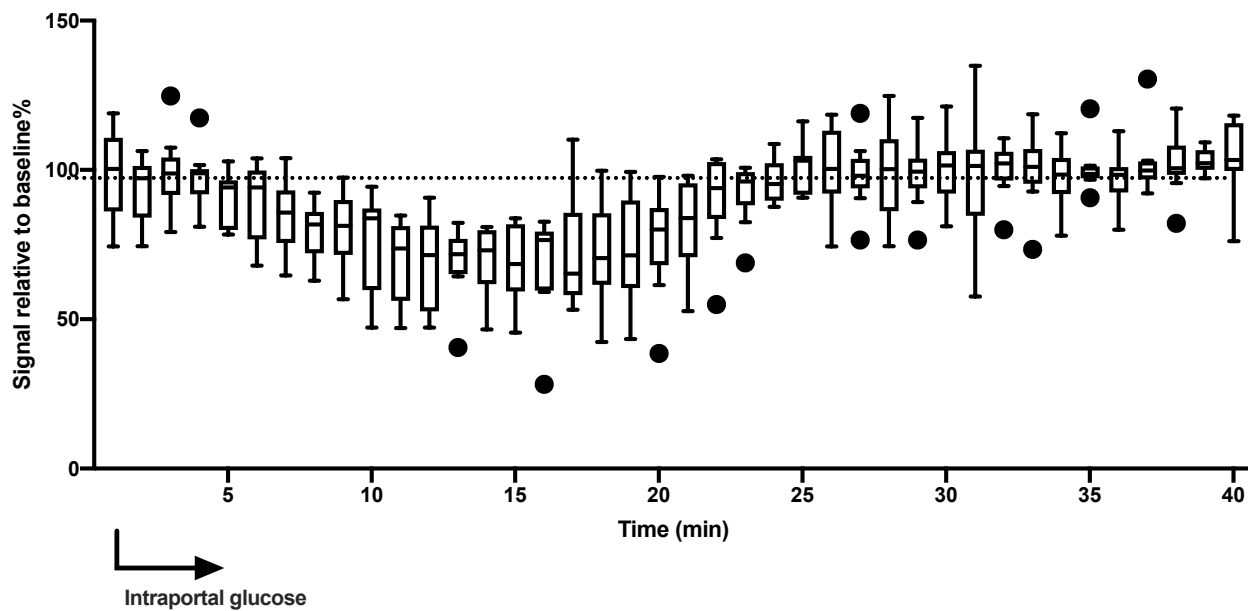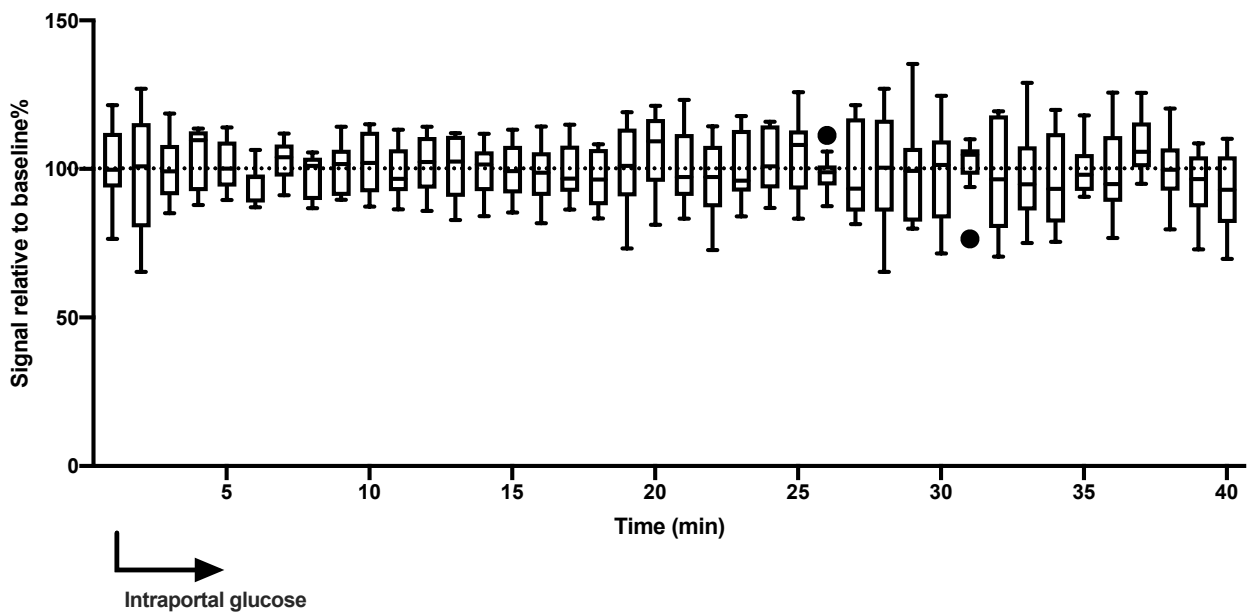
5 cm
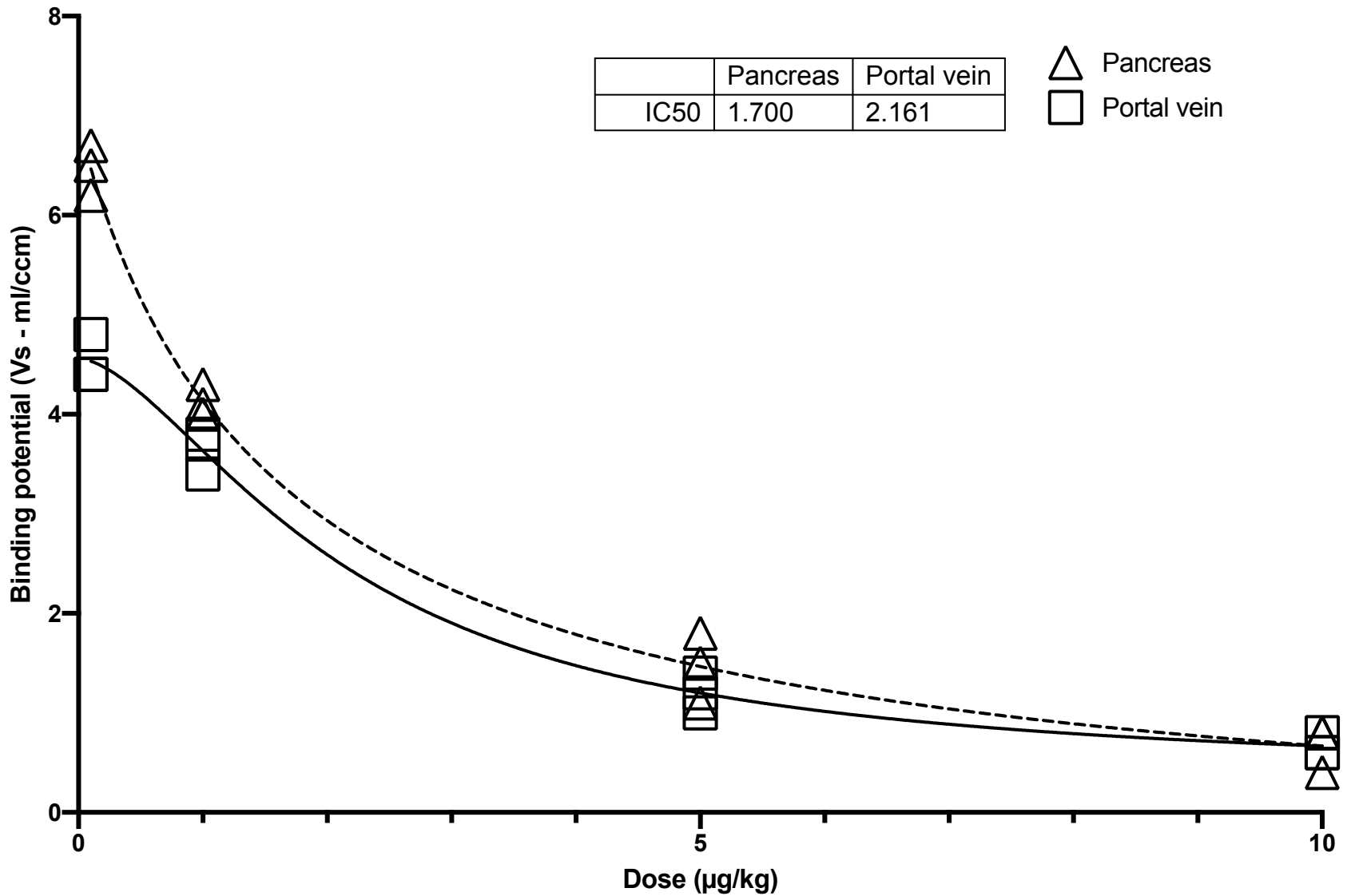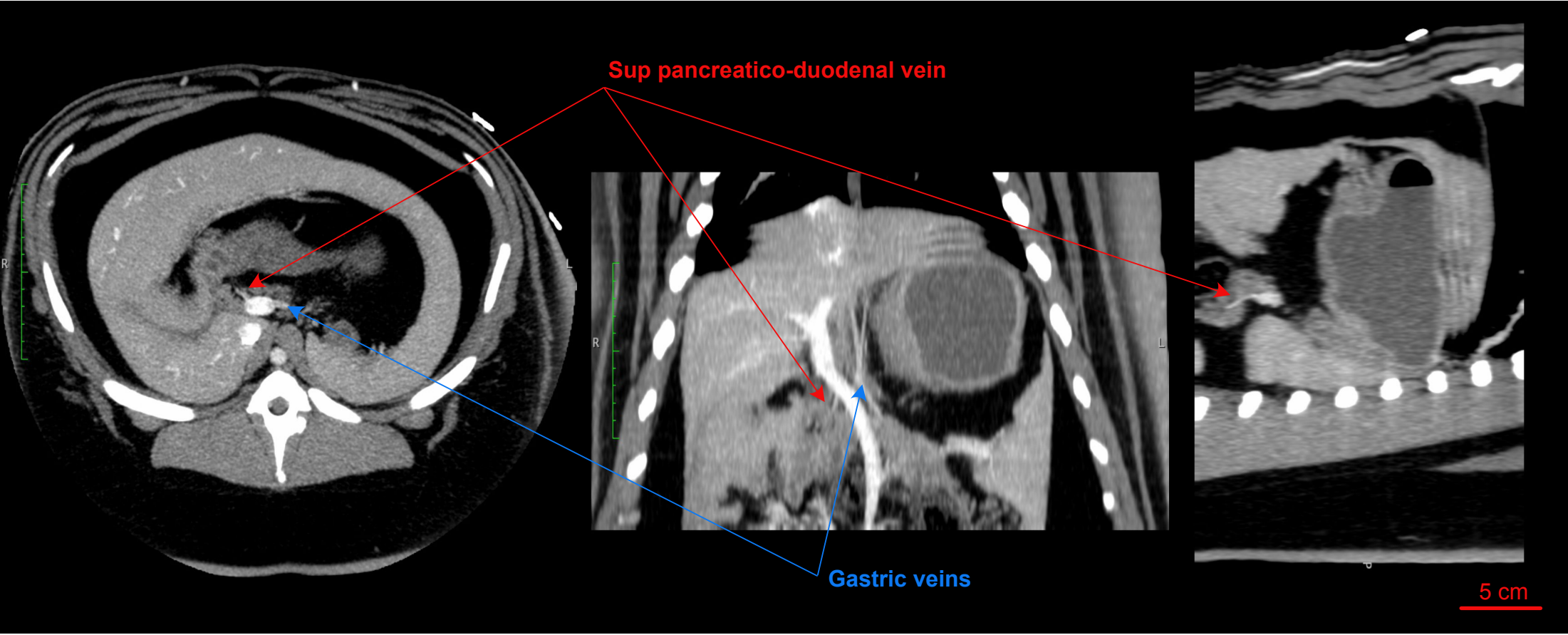
Supplemental Figure 1: Effect of escalating doses of cold DO3A-VS-Cys40-Exendin-4 on the binding potential of [68Ga]Ga-DO3A-VS-Cys40-Exendin-4 injected at 0.1 µg/kg. Data were obtained from three additional juvenile pigs explicitly used to validate the adequacy of the GLP-1r labeling at the portal area. Binding potentials were obtained from the compartmental analysis of the uptake extracted utilizing a volume of interest located on the portal vein which was itself identified using a co-registered CT image. The steady decrease of the binding potential with escalating dose demonstrates displacement of tracer and the specificity of its portal binding. All data points are presented on the graph, and superimposed data points could be present for some conditions.

Supplemental Figure 2: Example of raw portal time activity curve, whole blood radioactivity and the model adjustment for both. The plasma radioactivity used for model calculation is extrapolated from several discrete blood samples distributed to cover the whole imaging time. The insert represents the actual output of the radioactivity meter placed on the arterio-veinous loop. The raw blood signal is filtered using a software written under labview (Animate) then adjusted to a 3-exponential model (show in blue).

Supplemental Figure 3: Raw PET images (SUV color coded) of the abdomen at the portal vein level. The row represents the sum of the dynamic frames according to time. A gaussian filter (4mm kernel) was applied on all images set. The radioactivity spot observed at the bottom image of the lean animal is the top part of the kidney. The color coding is identical across the different recording time.

Supplemental Figure 4: Evoked potentials from portal afferent recorded at the cervical vagus in a single neuron recording setting. A. The capture of 10 consecutive electrical stimulation sweeps. The picture was obtained during a quiescent period of the afferent, an unusual feature for portal vagal afferents. B. The capture of 30 consecutive electrical stimulation sweeps. Unlike that in A, this afferent is spontaneously spiking. This results in superimposed spikes on several sweeps and represents a common recording condition for portal afferent. Note the slight reduction in temporal delay at the onset of the stimulation train that becomes negligible. Both A and B neurons have an estimated propagation speed of 1.8 m/sec and are classified as C neurons.

Supplemental Figure 5: Quantitative representation of the evolution of spiking activity during intraportal glucose infusion in lean and obese groups. The mean spiking activity over a

minute is presented using the whiskers and outliers Tukey method. The outliers are shown as black dots. Data are presented as percentage change relative to baseline immediately before the onset of portal injection. Note the clear spiking inhibition during intraportal glucose in the lean group only. Some individual data points are missing both in lean and obese group between 25 to 40 minutes as a consequence of temporary artefacts due to, operator dependent, minute suckling of the liquid produced by the nerve bundle under recording. This explain in part the larger stand art error during this period.

Supplemental Figure 6: Location of the superior pancreatico-duodenal vein in an obese pig obtained on an injected CT image. The superior pancreatico-duodenal vein connects to the portal vein at the same location as the gastric veins. Localization of the superior pancreatico-duodenal vein has been achieved adequately in 5 and 4 lean and obese animals, respectively, probably due to size/spatial resolution limitations. The figure overlaps four consecutive CT slices to allow for the identification of the venous structures.